PHYSICAL REVIEW A VOLUME 2, NUMBER 2 AUGUST 1970

Compton Scattering of X Rays from Bound Electrons

P. Eisenberger and P. M. Platzman
Bell Telephone Laboratories, Murray Hill, New Jersey 07974
(Received 9 January 1970)

Exact and approximate methods for determining the momentum distribution of electronic systems from Compton scattering measurements are presented. The method used previously to analyze Compton scattering measurements, the impulse approximation (IA), is derived from first principles, and its accuracy is compared with the exact calculations for Compton scattering from a hydrogenic system. It is shown that the IA gives very accurate results for weakly bound electrons and that exact calculation may only be necessary to subtract out the contributions to Compton scattering from deeply bound core electrons. Experimental results for Compton scattering from helium are presented as a test of the above ideas. Analyzing the results of the experiment in the IA gives a momentum distribution for the weakly bound helium electrons which is in excellent agreement with the momentum distribution obtained from Clementi Hartree-Fock wave functions.

1. INTRODUCTION

Following the discovery and explanation of the Compton effect,[1] it was suggested[2,3] that it would be useful for measuring the electronic momentum density (EMD) of electronic systems. Recently, there has been renewed interest in utilizing this rather unique microscopic probe.[4-8]

At present, all the experimental results have been analyzed utilizing a theory [impulse approximation (IA)] which assumes that the electrons which are doing the scattering may be treated as free rather than bound. The binding is included only in so far as it produces a spread of initial free electron energies or momenta. No rigorous theoretical justification for this approximation or its limits of validity has been given. In addition, all of the accurate experiments to date were performed on systems for which the uncertainty in the ground-state electronic wave function was large enough to preclude an "experimental" check of the IA.

In this paper, we intend to study the Compton scattering from an electron initially in a hydrogen $1s$ ground state with arbitrary Z.

The nonrelativistic Compton cross section may be written down exactly for this system. This calculation is outlined in Sec. II. In Sec. III, we will derive the so-called IA from first principles. Its limits of validity and the accuracy with which it describes the scattering from bound electrons will be clearly displayed.

It is well known that it is the outer or weakly bound electrons which are of greatest interest in solid-state and molecular physics. It will be shown that these outer electrons produce a scattered photon spectrum which, under the experimental conditions used by the recent investigators, is very accurately described by the IA. However, both in solids and molecules there is a scattered spectrum due to the tightly bound electrons which must be subtracted from the measured result to obtain information about the outer electrons. The results of our calculation clearly indicate the region of validity for using the IA to subtract out the core contributions as well as indicating the exact procedure that can be followed when the IA breaks down.

In Sec. IV, we will compare some experimental results obtained in He with the IA and with the very accurate and very well-known Hartree-Fock ground-state calculations for this system. The very good agreement obtained substantiates the theoretical calculations and indicates the potential of the Compton scattering technique.

II. HYDROGEN ATOM

Consider the incoherent scattering of x rays from a system containing electrons. Such a scattering process is shown schematically in Fig. 1. The incoming monochromatic x-ray beam is characterized by the frequency ω_1 and wave vector $\vec{k}_1$. The scattered x ray is characterized by the corresponding quantities ω_2 and $\vec{k}_2$. If the system is almost transparent to the incoming x-ray beam, i.e., only a small quantity is scattered into the final beam $\vec{k}_2$, then the scattering cross section may be completely characterized by the two quantities

$$\omega = \omega_1 - \omega_2, \quad \vec{k} = \vec{k}_1 - \vec{k}_2 . \tag{1}$$

In the x-ray region, one is typically concerned with values of $\omega_1 \sim 20$ keV and $k_1 = 2\pi/\lambda_1 \cong 10$ Å^{-1}. The values of these parameters imply that one may investigate the behavior of the scattering

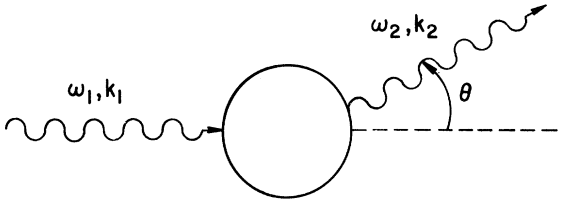

FIG. 1. Schematic diagrams of incoherent process.

cross section over a large portion of the ω, k plane.

Since the scattering is weak, we may calculate the cross section by using lowest-order Born approximation. Suppose the electronic system has a Hamiltonian of the form given by

$$H = p^2/2m + V(r) \equiv H_0 + V(r) \ . \tag{2}$$

The quantity $\vec{p}$ is the electron's momentum, and $V(r)$ is the external potential in which it moves, i.e., for the hydrogen atom $V(r) = -Ze^2/r$.

In order to find the coupling to the electromagnetic field, we replace, in the standard manner, $\vec{p}$ by $\vec{p} - e/c\vec{A}$. The coupling Hamiltonian below then contains two distinct types of terms:

$$H_c = e^2A^2/2mc^2 - e\vec{p}\cdot\vec{A}/mc \ . \tag{3}$$

To find the cross section for Compton scattering, we must go to second order in the vector potential $\vec{A}$, i.e., to first order in the A^2 term or second order in the $\vec{p}\cdot\vec{A}$ terms in Eq. (3). For unbound electrons $V(r) = 0$, all of the Compton scattering is given by the A^2 term in Eq. (3), i.e.,

$$\left(\frac{d\sigma}{d\Omega}\right)_{\rm Th} = \left(\frac{e^2}{mc^2}\right)^2 (\vec{\epsilon}_1\cdot\vec{\epsilon}_2)^2 \left(\frac{\omega_2}{\omega_1}\right)^2 \ . \tag{4}$$

In Eq. (4), the final frequency ω_2 is related by energy conservation to the initial frequency by

$$\omega_1 - \omega_2 = \hbar k^2/2m \ .$$

This A^2 or Thompson approximation can be shown to be accurate to quantities of order δ^R, where δ^R is given by

$$\delta^R \cong (\hbar\omega_1/mc^2)^2 \ . \tag{5}$$

When δ^R is not small compared to unity, one must go to a completely relativistic formulation, i.e., the Klein-Nishina formula.[9] One cannot patch up Eq. (4) by using the $\vec{p}\cdot\vec{A}$ terms.

For bound electrons, the $\vec{p}\cdot\vec{A}$ terms in Eq. (3), taken in second order, can be important. For the values of ω_1 which are used in Compton scattering experiments, it will be shown in the Appendix that they are *not* significant. In the ensuing treatment, we will *only* discuss the contributions to the Compton cross section from the A^2 term in lowest-order perturbation theory. In this approximation the cross section for a one-electron atom may be written[10]

$$\frac{d\sigma}{d\Omega d\omega} = \left(\frac{d\sigma}{d\Omega}\right)_{\rm Th}\left(\frac{\omega_1}{\omega_2}\right) \times \sum_j \overline{\sum_i} \left|\langle f| e^{+i\vec{k}\cdot\vec{r}}|i\rangle\right|^2 \delta(E_f - E_i - \omega). \tag{6}$$

For the hydrogen atom, the final-state wave function for an electron in the continuum is given by

$$|f\rangle = (2\pi/pa)^{1/2}(1 - e^{-2\pi/pa})^{-1/2} \times e^{i\vec{p}\cdot\vec{r}} F(i/pa, 1, i(pr - \vec{p}\cdot\vec{r})) \ , \tag{7}$$

with $E_f = p^2/2m$.

In Eq. (7) the function F is the standard confluent hypergeometric function. The initial state in Eq. (6) is simply the 1s hydrogenic ground state with energy $-|E_B|$. For transitions to the continuum, the sum over final states is replaced by an integral over the wave vector $\vec{p}$, i.e.,

$$\sum_f \to \int \frac{d^3p}{(2\pi)^3} \ . \tag{8}$$

The square of the matrix element in Eq. (6) may be evaluated exactly; it is given by[11]

$$|M_{fi}|^2 \equiv \left|\langle f|e^{i\vec{k}\cdot\vec{r}}|i\rangle\right|^2 = \left(\frac{\pi^2 8^3}{a^6 p}\right) \times \left(1 - e^{-2\pi/pa}\right)^{-1} \exp\left[\frac{-2}{pa}\tan^{-1}\left(\frac{2Bp}{k^2 + B^2 - p^2}\right)\right] \times [B^2 + (\vec{p} - \vec{k})^2]^{-4}[(\vec{k}\cdot(\vec{k} - \vec{p}))^2 + (\vec{p}\cdot\vec{k}/pa)^2] \times [(k^2 - p^2 + B^2)^2 + 4p^2B^2]^{-1} \ , \tag{9}$$

where $B \equiv 1/a = Zme^2/\hbar^2$.

Averaging Eq. (9) over the *directions* of p, one finds that

$$\langle |M_{fi}|\rangle^2 = \frac{\pi^2 8^3 a^2}{p}(1 - e^{-2\pi/pa})^{-1} \times \exp\left[\frac{-2}{pa}\tan^{-1}\left(\frac{2pa}{1 + k^2a^2 - p^2a^2}\right)\right] \times [k^4a^4 + \tfrac{1}{3}k^2a^2(1 + p^2a^2)] \times [(k^2a^2 + 1 - p^2a^2)^2 + 4p^2a^2]^{-3} \ . \tag{10}$$

The cross section is now found by simply inserting Eq. (10) into Eq. (6) and fixing the magnitude of p from the energy-conservation δ function, i.e.,

$$p^2/2m = -|E_B| + \omega \ . \tag{11}$$

If we assume that the energy and momentum transfer involved in the x-ray scattering are large relative to the characteristic energy and momentum of the bound state, then the wave vector p of the final-state electron is a large quantity, and we may expand Eq. (10) as a power series in $(pa)^{-1}$. If we do this, we arrive at an expression for the cross section

$$\frac{d\sigma}{d\omega d\Omega} \sim \frac{\omega_2}{\omega_1 k(1+v^2)^3}\left(1+\frac{2}{pa}\tan^{-1}(v)+\frac{3}{2}\frac{v}{pa}\right), \tag{12}$$

where $v = a|k-p|$.

Equation (12), apart from the ω_2/ω_1 factor, is close to but not exactly the same as the formula derived by Bloch.[12] There are, apparently, some small numerical errors in this early calculation.

The details of the expansion are not very important. What is important, however, is that it is clear from examining the exact expression [Eq. (10)] that an expansion in powers $(pa)^{-1}$ is not a very good approximation. There are correction terms to Eq. (12) which are of order $2\pi/pa$. Under typical experimental conditions, this quantity is not particularly small.

For the moment, let us leave our exact expressions Eqs. (6)–(10) and their expanded version Eq. (12) and go on to a derivation of the IA. Having derived the IA, we will then return to our exact formula and make a detailed numerical comparison between it and the IA. The IA will turn out to be a much more accurate approximation to the exact expression than the expansion given in Eq. (12).

III. IMPULSE APPROXIMATION

In this section, we will develop an approximation scheme for the exact expression given by Eqs. (6) and (10). This approximation will be shown to be valid for large electron recoil energies, i.e., $\omega \gg E_B$.

The exact nonrelativistic formula [Eq. (6)] may be rewritten. In Eq. (6), we replace the δ function by its Fourier representation, i.e.,

$$\delta(\omega-(E_f-E_i)) \equiv (1/2\pi)\int_{-\infty}^{+\infty} e^{i[\omega-(E_f-E_i)]t}\,dt \ . \tag{13}$$

The exponentials are replaced by the Hamiltonian operator acting on the appropriate eigenfunction, i.e.,

$$e^{iHt}|i\rangle = e^{iE_it}|i\rangle \ . \tag{14}$$

Using Eqs. (13), (14), we may simply rewrite Eq. (6) as

$$\frac{d\sigma}{d\Omega d\omega} = \left(\frac{d\sigma}{d\Omega}\right)_{\rm Th}\frac{\omega_1}{\omega_2}\frac{1}{(2\pi)}\int dt e^{i\omega t} \times \langle i|e^{iHt}e^{-i\vec{k}\cdot\vec{r}}e^{-iHt}e^{+i\vec{k}\cdot\vec{r}}|i\rangle = \left(\frac{d\sigma}{d\Omega}\right)_{\rm Th}\frac{\omega_1}{\omega_2}\,S(k,\omega) \ . \tag{15}$$

The Hamiltonian operator (e^{iHt}) may be expanded using a well-known theorem as

$$e^{iHt} = e^{iH_0t}e^{iVt}e^{-[H_0,V]t^2/2}\cdots \ . \tag{16}$$

The higher-order terms in Eq. (16) involve multiple commutators, and are higher order in powers of the time t. If we reexamine Eq. (15), we immediately see that those times which are of importance in the integration are of order ω^{-1}. When ω is much larger than all of the other characteristic energies associated with the ground state of the electron, one can set

$$\exp(-\tfrac{1}{2}[H_0,V]t^2) \equiv 1 \ . \tag{17}$$

Equation (17) is the essence of the IA.[13] Our expansion, Eq. (16), is essentially an expansion in powers of the time t. We will see how good an approximation this is shortly. If we drop the commutator in Eq. (16), then Eq. (15) may be rewritten as

$$S^{\rm I}(k,\omega) = (1/2\pi)\int_{-\infty}^{+\infty} dt e^{i\omega t} \times \langle i|e^{iH_0t}e^{iVt}e^{-i\vec{k}\cdot\vec{r}}e^{-iVt}e^{-iH_0t}e^{+i\vec{k}\cdot\vec{r}}|i\rangle \equiv \int dt e^{i\omega t}F_k(t) \ . \tag{18}$$

Since $V(r)$ commutes with $\vec{r}$, the quantity e^{iVt} may be commuted through the e^{ikr}, and we obtain

$$S^{\rm I}(k,\omega) = (1/2\pi)\int_{-\infty}^{+\infty} e^{i\omega t} \times \langle i|e^{iH_0t}e^{-i\vec{k}\cdot\vec{r}}e^{-iH_0t}e^{+i\vec{k}\cdot\vec{r}}|i\rangle \ . \tag{19}$$

The potential V has *vanished* from our approximate expression [Eq. (19)] for the scattering cross section. Although it looks as if we have completely neglected V, the physics of the situation tells us that we have not neglected it, but that the V has cancelled out of the energy for the initial and final states. This is the central feature of the IA. For short times, the potential that the electron is moving in may be thought of as a constant. The energy of the electron is measured, in both the initial and final states, relative to this constant instantaneous potential.

Equation (19) is now simply evaluated by inserting a complete set of states which are eigenfunctions of H_0. These states are simply the usual plane-wave momentum eigenfunctions. The integral over t is then easily performed, and we find that

$$S^{I}(k;\omega) = \int \frac{d^3p_0}{(2\pi)^3} |f(p_0)|^2 \, \delta\left(\omega - \frac{k^2}{2m} - \frac{\vec{k}\cdot\vec{p}_0}{m}\right). \quad (20)$$

The quantity $f(p_0)$ is the Fourier transform of the ground-state wave function $\varphi_0(x)$, i.e.,

$$f(p_0) = \int e^{i\vec{p}_0\cdot\vec{r}} \varphi_0(r)\, d^3r \, . \quad (21)$$

Equation (20) is what one would have obtained if one had assumed that the initial state of the electron was one with momentum p_0 and energy $p_0^2/2m$, not $-|E_B|$. The energy δ function tells us that the scattered photon is shifted in frequency both by the momentum transfer term $k^2/2m$ and the doppler shift component $(\vec{k}\cdot\vec{p}_0/m)$. Thus in the IA, the essential nature of the Compton scattering process is clearly revealed to be a doppler broadening of the scattered photon energy. The spectrum of the scattered photons is simply related to the distribution of momenta in the physical system by Eq. (20). The function $|f(p_0)|^2$ gives the probability of finding the initial electron with a given momentum p_0. The integral in Eq. (20) essentially states that at each k, ω, the scattered intensity is proportional to the number of electrons having a fixed value of momentum in the direction of the photon's scattering vector $\vec{k}$. The value of the momentum projection is fixed by the energy δ function in Eq. (20).

IV. VALIDITY OF IMPULSE APPROXIMATION

Before making a numerical comparison between the IA and the exact calculation for our model hydrogenic system, a general evaluation of the accuracy of IA is supplied by comparing moments of $S(\vec{k}, \omega)$ for the two approaches. Since we have

$$S(k,\omega) = (1/2\pi) \int_{-\infty}^{+\infty} e^{i\omega t} F_k(t)\, dt \, , \quad (22)$$

the frequency moments for fixed k are given by

$$S_n(k) \equiv \int d\omega\, \omega^n S(k,\omega) = i^{n-1} F_k^{n-1}(0) \, . \quad (23)$$

Here F_k^n is the nth time derivative of $F_k(t)$.

The first four moments $n \leq 3$ are easily computed for the *exact* Hamiltonian H [Eq. (2)]. After a good deal of algebra, we find that

$$\int_{-\infty}^{+\infty} d\omega\, S(k,\omega) = 1 \, , \quad (24)$$

$$\int_{-\infty}^{+\infty} d\omega\, \omega S(k,\omega) = k^2/2m \, , \quad (25)$$

$$\int_{-\infty}^{+\infty} d\omega\, \omega^2 S(k,\omega) = \left(\frac{k^2}{2m}\right)^2 + \frac{4}{3}\left(\frac{k^2}{2m}\right)\left\langle \frac{p^2}{2m}\right\rangle \, , \quad (26)$$

$$\int_{-\infty}^{+\infty} d\omega\, \omega^3 S(k,\omega) = \left(\frac{k^2}{2m}\right)^3 + 4\left(\frac{k^2}{2m}\right)^2 \left\langle \frac{p^2}{2m}\right\rangle + \tfrac{2}{3}(k^2/2m)\langle \nabla^2 V\rangle/2m \, . \quad (27)$$

Equations (24)–(27) are correct independent of the explicit form of the *one*-electron potential $V(r)$. The expectation value of $p^2/2m$ and $\nabla^2 V(r)$ is taken in the ground state. The details of this evaluation are not essential to the argument.

In the derivation of the IA, it was clearly shown that the form of $S(k, \omega)$ is the same as in the exact expression [Eq. (15)] except that the potential $V(r)$ is absent (i.e., $H \to H_0$). In other words, for the IA one can evaluate Eq. (23) for the nth moment with a Hamiltonian which only contains the kinetic energy. In this case, all terms in the various moments which are proportional to the potential energy will be identically zero. Thus, moments zero through two will be identical in the two calculations, while the third moment will differ by the last term in Eq. (27).

In the limit of large recoil energy, the error in the third moment S_3 is given by

$$\frac{S_3 - S_3^I}{S_3} \cong \frac{\frac{2}{3}(k^2/2m)\langle \nabla^2 V\rangle/2m}{(k^2/2m)^3} \, . \quad (28)$$

For the hydrogen atom, Eq. (28) is easily evaluated, and we find a relative error in the third moment for large k which is

$$(S_3 - S_3^I)/S_3 \cong \tfrac{8}{3}(E_B/E_R)^2 \, , \quad (29)$$

where $E_R \equiv k^2/2m$. (30)

In order to see, in more detail, how good a characterization the IA is, we will go to a detailed numerical comparison in hydrogen. Before doing this, however, we would like to make two points relating to the exact and approximate forms of the moments of the distribution function.

(i) The moments given in Eqs. (24)–(27) are frequency moments for fixed momentum transfer k. This is *not* equivalent to integrating over the outgoing frequency of the photon for a fixed angle. In the experiment, as we scan across the line, for fixed scattering angle, the k vector changes. This implies that we make errors in computing the moments from the experimental data which are of order ω/ω_1. In a given situation these errors may be significant and in principle corrections should be made.

(ii) The sum rules given in Eqs. (24)–(27) have contributions from the bound-state terms as well as the continuum (i.e., the final electron state can be a discrete bound state as well as the continuum). For pure A^2 coupling, the bound-state contributions to cross section involve matrix elements of the form

$$M_{ni} = \langle n | e^{i\vec{k}\cdot\vec{r}} | i\rangle \, . \quad (31)$$

Here the quantity $|n\rangle$ is some excited bound hy-

drogenic state.

A general expression for the cross section for the discrete transition for our hydrogenic system is given by[14]

$$\left(\frac{d\omega}{d\omega\, d\Omega}\right)_D = \left(\frac{d\sigma}{d\Omega}\right)_{\mathrm{Th}} \left(\frac{2}{3}\right)^8 \frac{(ka)^2}{n^3} \left(3(ka)^2 + \frac{(n^2-1)}{n^2}\right) \times \frac{[(n-1)^2/n^2 + (ka)^2]^{n-3}}{\{[(n+1)/n]^2 + (ka)^2\}^{n+3}} \,. \tag{32}$$

In Eq. (32), n is the principal quantum number. A special case of this is when $n = 1$, which corresponds to Rayleigh or elastic scattering, such that

$$\left(\frac{d\sigma}{d\omega\, d\Omega}\right)_R = \left(\frac{d\sigma}{d\Omega}\right)_{\mathrm{Th}} [1 + (\tfrac{1}{2}ka)^2]^{-4} \,. \tag{33}$$

One immediately notes that for $ka > 1$ both the Rayleigh and Raman components decrease as $(1/ka)^8$, and thus for $ka \geq 2$, they will not make a significant contribution to the total scattered in-

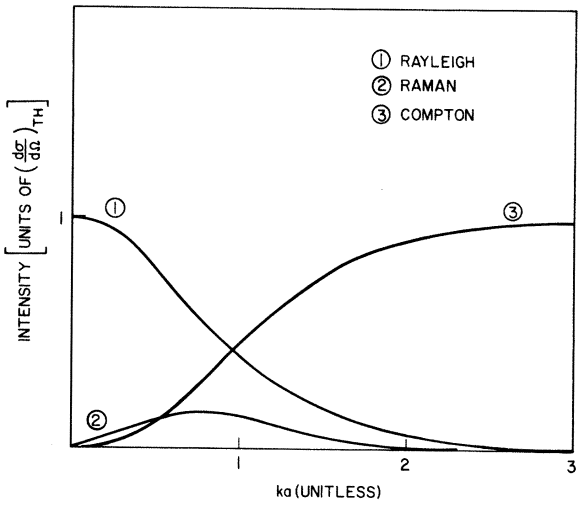

FIG. 2. Compton, Rayleigh, and Raman cross sections as a function of ka.

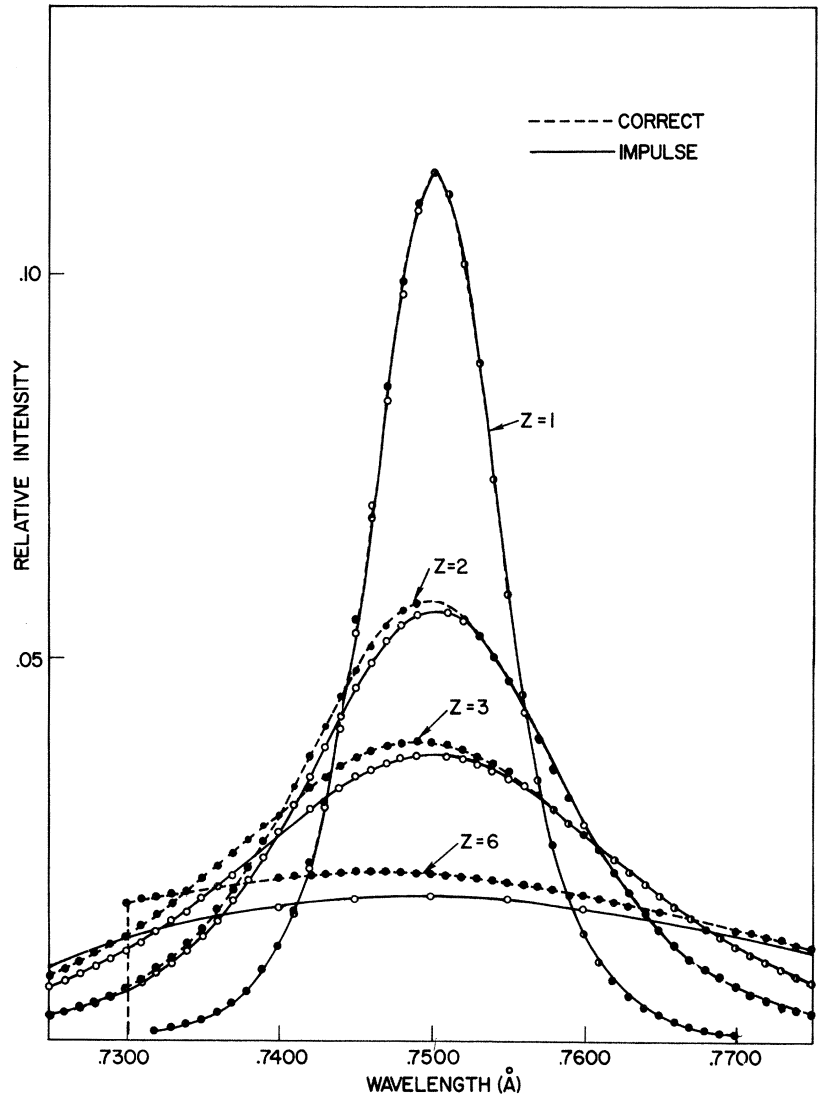

FIG. 3. Compton spectrum for hydrogenic systems with different Z's. A comparison between the results of the exact calculation [Eq. (11)] and the IA [Eqs. (15) and (20)] for Mo K_{α_1} radiation ($\omega_1 \cong 17.4$ keV and $E_R \sim 940$ eV).

tensity. In Fig. 2, we have indicated how the various contributions to the total scattered intensity vary as a function of ka.

Figure 3 gives the Compton spectrum for hydrogenic systems with different Z's. The dotted curves are the exact results. The solid curves were obtained by using the IA results [i.e., substituting Eq. (20) in Eq. (15)]. In Fig. 3, the incident x-ray energy is 17.4 keV; the angle between the incident and scattered beams is 133.75°; and the recoil energy at the center of the line is approximately 940 eV. The trend is clear. The long wavelength large recoil portion of the spectrum is given extremely accurately by the IA. As one approaches threshold $\omega \cong E_B$, the deviations become larger. For the high side of the line, $\omega > k^2/2m$, the IA holds uniformly to something of order $(E_B/E_R)^2$.

There is an interesting phenomenon associated with the threshold behavior of curves given in Fig. 3. The cross section at threshold is a constant and not proportional to the square root of the energy above threshold. The reason for this may be found by examining the exact final-state wave function given in Eq. (6). As the kinetic energy of the final electron goes to zero (i.e., $p \to 0$),

$$|p\rangle \sim p^{1/2} e^{i\vec{p}\cdot\vec{r}} \quad . \tag{34}$$

The normalization of the wave function blows up in just such a way as to cancel the density-of-states factor present in the cross section. This so-called Sommerfeld correction to the wave function is a well-known effect. The IA neglects it entirely. In practice, no sharp discontinuity need be observed because the discrete transitions whose cross sections were given in Eq. (32) will have intensities comparable to transitions to the continuum.

In Fig. 4, we have taken a higher value for the energy of incident x-rays (59.3 keV). The recoil energy at the center of the line is ~ 9.7 keV. The cross sections are evaluated in this case, and we see that the IA is a still more accurate description of the cross section.

In summary, the IA seems to be very good. It can be used with a confidence determined solely by the parameter $(E_B/E_R)^2$.

To this point we have concentrated our attentions on the IA and its application to a simple one-electron hydrogenic atom. This kind of technique can be applied in a straightforward manner to more complicated many-electron systems. The operator $e^{i\vec{k}\cdot\vec{r}}$ for many electrons is replaced by a sum of the contributions from the different electrons, i.e.,

$$\rho_k = \sum_{\vec{r}_i} e^{i\vec{k}\cdot\vec{r}_i} \quad . \tag{35}$$

In second-quantized notation, the density operator ρ_k given in Eq. (35) may be written

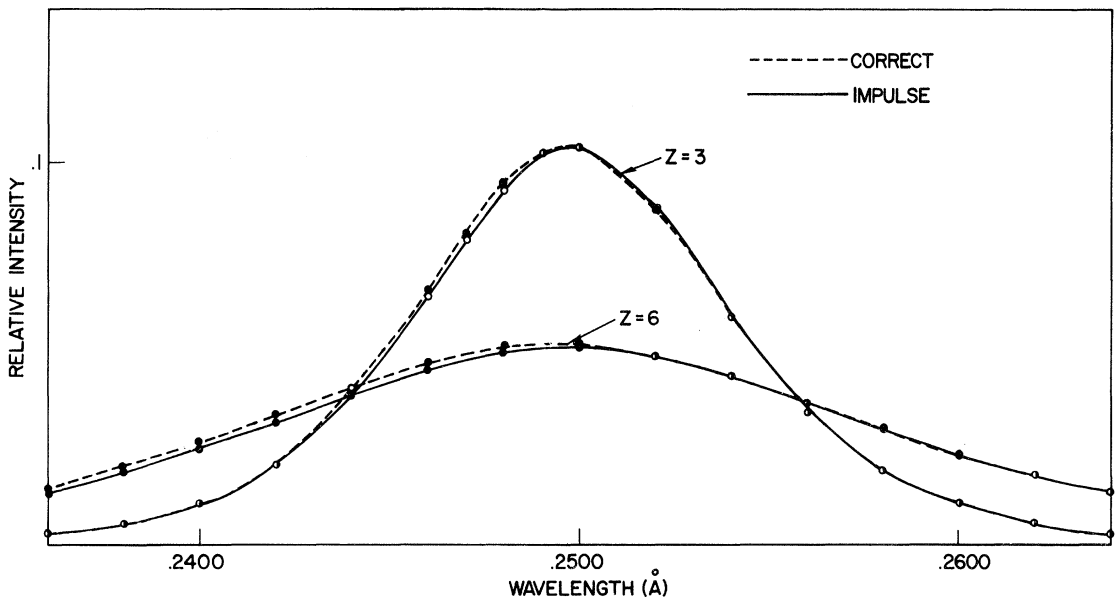

FIG. 4. Compton spectrum for hydrogen systems with different Z's, for tungsten K_{α_1} radiation ($\omega_1 \cong 59.3$ keV and $E_R \sim 9.7$ keV).

$$\rho_k(0)=\sum_{p_0} a^+_{p_0+k}\, a_{p_0} \quad , \tag{36}$$

where a^+ and a are *the* standard creation and annihilation operators, respectively.

In the IA, the Compton cross section from an atom containing many electrons, one neglects all commutators of the kinetic and potential energies. The result for the cross section is then simply given by[8]

$$\frac{d\sigma}{d\omega\, d\Omega}=\left(\frac{d\sigma}{d\Omega}\right)_{\mathrm{Th}}\frac{\omega_1}{\omega_2}\frac{1}{(2\pi)^3} \times\int \delta\left(\omega-\frac{k^2}{2m}-\frac{\vec{k}\cdot\vec{p}_0}{m}\right) n_{p_0}\, d^3p_0$$

$$\equiv\left(\frac{d\sigma}{d\Omega}\right)_{\mathrm{Th}}\frac{\omega_1}{\omega_2}J(q), \tag{37}$$

where $n_{p_0}=\langle a^+_{p_0} a_{p_0}\rangle$, (38)

and $q=\hat{k}\cdot\vec{p}_0$. (39)

Equation (37) is directly analogous to Eq. (20); the only difference is that the Fourier transform of the one-electron wave function has been replaced by the probability of finding an electron with momentum p_0, i.e., n_{p_0}.[8]

V. EXPERIMENTAL RESULTS OF HELIUM

Compton scattering experiments were performed on liquid helium using 0.7093-Å molybdenum radiation. The details of the experiment parallel closely those used by Phillips and Weiss[4] and will be described shortly in a subsequent publication.[15] In Fig. 5 we show the experimental Compton profile for helium. About 10^4 counts were obtained at the peak. This profile is obtained from the measured spectrum by subtracting the low background (less than 3%) and performing the Rachinger process[4] to separate out the K_{α_1} and K_{α_2} components.

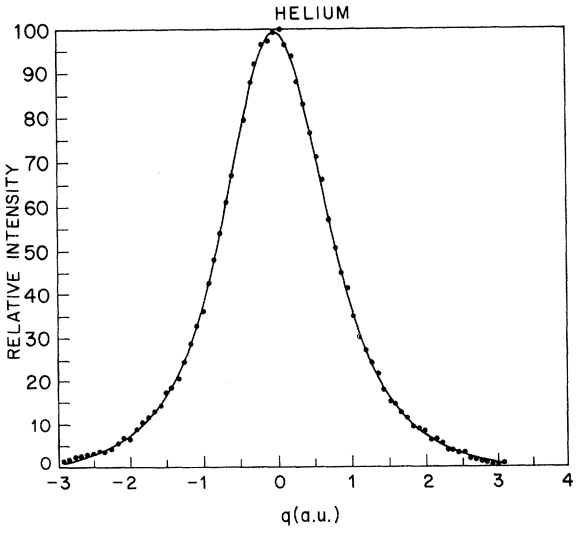

FIG. 5. Experimental Compton profile for helium. The variable q is equal to the projection of the electrons momentum $\vec{p}_0$ on the scattering vector $\vec{k}$.

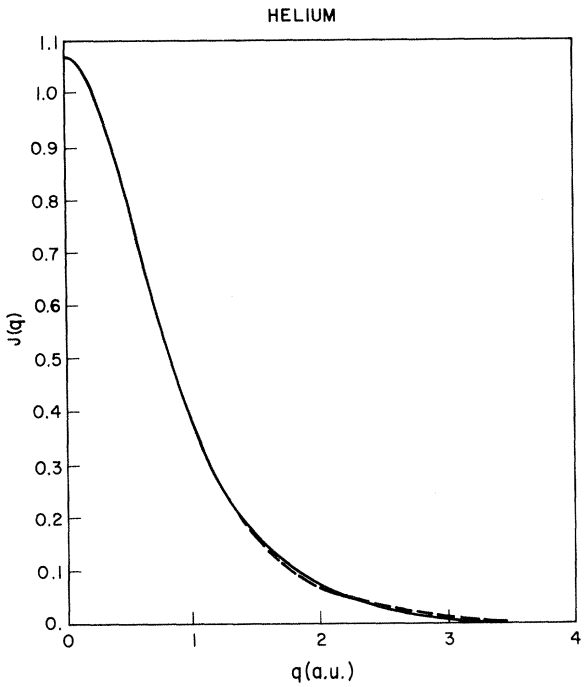

FIG. 6. Comparison of experimental Compton profile and that calculated by the IA. The areas under the two were made equal to 2, the number of electrons per atom in helium. The solid line is the experimental profile, and the calculated profile is the dotted line.

The wavelength of scattered radiation was determined by Bragg scattering from the LiF(400) reflection. The projection of the electron's initial momentum on the scattering vector $\vec{k}$ (the parameter q) is determined by the relationship between it and the scattered wavelength implied by the δ function in Eq. (37). It is the parameter q which is used in Fig. 5. A resolution correction is perfomed on the data shown[4] in Fig. 5 and the resulting experimental profile is plotted in Fig. 6 as the solid line. In that plot $J(q)$ has the meaning indicated in Eq. (37).

Using Eq. (37) together with a Clementi[16] Hartree-Fock wave function, a theoretical Compton profile is easily calculated.[17] In the Hartree-Fock approximation the wave function is a simple antisymmetrized product of one-electron wave functions. The scattering takes place from the two bound electrons separately. Thus, the "many-body" Compton profile [Eq. (37)] for helium is nothing more than the single-electron profile Eqs. (15), (20), and (21) multiplied by a factor of

2. The resulting $J(q)$ as calculated in the IA for helium is plotted as the dotted line in Fig. (6) for comparison with the experiment. Over most of the curve the two agree to better than graphical accuracy. Over the whole curve the two agree within the experimental error, which is 1% at the peak.

The above results clearly support the theoretical conclusion that for weakly bound electrons the IA is very accurate. For deeply bound core electrons it will probably be necessary to make exact calculations. These will probably entail numerical integration of Eq. (6).[18] For most ground-state wave functions there is no closed-form expression for the appropriate matrix elements.

The high possible experimental accuracy of the Compton scattering probe will undoubtedly result in the use of corrections to the IA for the deeply bound electrons. However, because the more deeply bound electrons have a very flat and broad momentum distribution, it will be possible to obtain considerably higher accuracy for the sharp momentum spectrum of the weakly bound electrons without worrying too much about a very accurate momentum distribution for the core electrons.

ACKNOWLEDGMENTS

Thanks are given to M. Lax for many conversations concerning the IA and the nature of the hydrogenic matrix elements. We would also like to thank B. Hennecker for supplying his calculations of the Compton profile for helium. The help of R. Weiss in the initial stages of the Compton study is gratefully acknowledged. The technical assistance of W. Marra was greatly appreciated.

APPENDIX

In this Appendix, we would like to estimate the importance of the $\vec{p}\cdot\vec{A}$ terms in the x-ray scattering from electrons in solids.

From Eq. (3), the coupling of x rays to the electronic system can be written as

$$H_c = e^2A^2/m + e\,\vec{p}\cdot\vec{A}/m \quad . \tag{A1}$$

The complete second-order matrix element which describes the nonrelativistic Compton scattering is shown graphically in Fig. 7. The solid lines represent the electronic system, and the wiggly lines the incoming and outgoing photons. Analytically, this complete matrix element may be written

$$M_{fi} = \frac{2\pi}{(\omega_1\omega_2)^{1/2}} r_0 \Bigg[\langle f | e^{+i\vec{k}\cdot\vec{r}} | i\rangle \, (\epsilon_1\cdot\epsilon_2) + \sum_n \frac{1}{m} \Bigg(\frac{\langle f | \vec{\epsilon}_2\cdot\vec{p}\, e^{-i\vec{k}_2\cdot\vec{r}} | n\rangle \langle n | \vec{p}\cdot\vec{\epsilon}_1 e^{+i\vec{k}_1\cdot\vec{r}} | i\rangle}{E_n - E_0 + \omega_1}$$

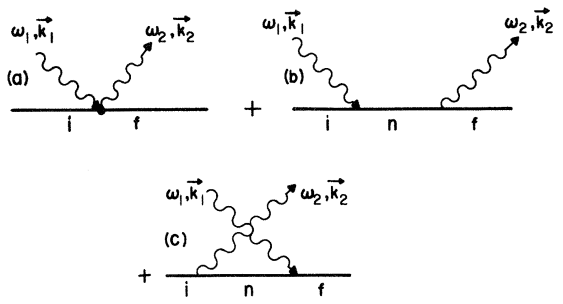

FIG. 7. Three scattering diagrams which contribute to the Compton scattering of low-energy x rays. (a) is the A^2 piece while (b) and (c) are the two pieces which come from the $\vec{p}\cdot\vec{A}$ terms in the coupling Hamiltonian.

$$+ \frac{\langle f | \vec{\epsilon}_1\cdot\vec{p}\, e^{+i\vec{k}_1\cdot\vec{r}} | n\rangle \langle n | (p\cdot\epsilon_2)\, e^{-i\vec{k}_2\cdot\vec{r}} | i\rangle}{E_n - E_0 + \omega_2} \Bigg) \Bigg] \quad . \tag{A2}$$

The first term in (A2) is simply the A^2 piece, i.e., Fig. 7(a). The last two are the contributions from the $\vec{p}\cdot\vec{A}$ terms, i.e., Fig. 7(b) and 7(c).

If ω_1 and ω_2 are much greater than $E_n - E_0$ then we may approximate M_{fi} by

$$M_{fi} \sim \langle f | e^{-i\vec{k}\cdot\vec{r}} | i\rangle \left(1 + \frac{p_f p_i}{m} \frac{\omega_1 - \omega_2}{(\omega_1\,\omega_2)} \right) \quad . \tag{A3}$$

In (A3), all polarization factors have been dropped.

One notes immediately that for a free stationary electron the $\vec{p}\cdot\vec{A}$ correction term is zero (i.e., $p_i = 0$). The $\vec{p}\cdot\vec{A}$ correction term [the second part of (A3)] can be rewritten as

$$\delta^{\vec{p}\cdot\vec{A}} \cong \frac{\hbar\omega_1}{mc^2} \left(\frac{E_B mc^2}{\hbar^2\omega_1^2} \right)^{1/2} \sin^{3/2}(\tfrac{1}{2}\theta) \, , \tag{A4}$$

where θ is the angle between the incident and scattered photon. The $\vec{p}\cdot\vec{A}$ correction terms can now be compared with the two other known types of correction to the x-ray scattering expressions given by Eq. (20). Relativity contributes a correction form given by Eq. (5), i.e.,

$$\delta \cong \left(\frac{\hbar\omega_1}{mc^2} \right)^2 \sin^2(\tfrac{1}{2}\theta) \quad . \tag{A5}$$

Corrections to the IA are, as we have seen, given by

$$\delta \cong \left(\frac{E_B}{\hbar\omega_1} \right)^2 \left(\frac{mc^2}{\hbar\omega_1} \right)^2 \frac{1}{\sin^2(\frac{1}{2}\theta)} \quad . \tag{A6}$$

A comparison of the above corrections clearly indicate that one cannot simply improve the IA measurements by using higher incident energies. Even though the correction to the IA is *decreasing*, the relativistic and $\vec{p}\cdot\vec{A}$ corrections are *increasing*. It is also clear from Eqs. (A4)–(A6)

that the $\vec{p}\cdot\vec{A}$ correction is never the largest one. This is of course only true when $E_B \ll \hbar\omega_1$. For $\hbar\omega_1 \sim E_B$ a resonance can occur in the $\vec{p}\cdot\vec{A}$ terms which will make it dominant.

A final remark concerning the $\vec{p}\cdot\vec{A}$ contribution to the Rayleigh and Raman terms discussed in Sec. IV is warranted. The same conditions hold for those transitions. If $ka \leq 1$ but ω_1, $\omega_2 \gg E_B$, the pure A^2 terms will dominate the Raman and Rayleigh cross sections. If, however, $\omega_1\ \omega_2 \sim E_B$, then the $\vec{p}\cdot\vec{A}$ terms will make the dominant contribution as they do in scattering experiments performed using lasers operating at visible wavelengths.

[1]A. H. Compton, Phys. Rev. 21, 484 (1923).
[2]J. W. H. Dumond, Phys. Rev. 33, 643 (1929).
[3]J. W. H. Dumond, Phys. Rev. 36, 146 (1930).
[4]W. Phillips and R. J. Weiss, Phys. Rev. 171, 790 (1968).
[5]M. Cooper and J. A. Leake, Phil. Mag. 15, 1201 (1967).
[6]R. J. Weiss and W. Phillips, Phys. Rev. 176, 900 (1968).
[7]A. Theodossious and P. Vosnidis, Phys. Rev. 145, 758 (1966).
[8]P. M. Platzman and N. Tzoar, Phys. Rev. 139, 410 (1965).
[9]J. M. Jauch and F. Rohrlich, *The Theory of Photons and Electrons* (Addison-Wesley, Cambridge, Mass., 1955).
[10]We will use units in which $\hbar = c = 1$, and the material is a unit volume.
[11]A. Gummel and M. Lax, Ann. Phys. (N.Y.) 2, 28 (1957).
[12]F. Bloch, Phys. Rev. 45, 674 (1934).
[13]G. F. Chew and G. C. Wick, Phys. Rev. 83, 636 (1952).
[14]P. Schnait, Ann. Physik 21, 90 (1934).
[15]P. Eisenberger (unpublished).
[16]E. Clementi, IBM J. Res. Develop. Suppl. 9, 2 (1965).
[17]B. Hennecker (private communication).
[18]Such calculations are being performed by C. DeCicco (report of work prior to publication).

PHYSICAL REVIEW A VOLUME 2, NUMBER 2 AUGUST 1970

Relative Orbital and Magnetic Substate Amplitudes in Single-Foil Excitation of Fast Hydrogen Atoms*

I. A. Sellin, J. A. Biggerstaff, and P. M. Griffin
Oak Ridge National Laboratory, Oak Ridge, Tennessee 37830
(Received 29 January 1970)

Within the limits set by our experimental apparatus, large-amplitude zero-field oscillations of H fine-structure amplitudes treated in a recent letter of Macek were not observed in polarization–versus–flight-path measurements on H_β, H_γ, and Ly_α emissions from suddenly excited H atoms (50- and 150-keV incident protons). Random initial phases for orbital and magnetic substates and approximately equal magnetic substate populations are indicated, in contrast to binary electron capture in gases. A successful test of the theoretical polarization of 2*s* Stark quench radiation was also made.

INTRODUCTION

Several interesting suggestions for exploiting coherent emission effects stemming from zero-field oscillations of H fine-structure (fs) amplitudes in fast-beam experiments were made in a recent letter of Macek.[1] Briefly, atoms are impulsively excited ($\sim 10^{-14}$-sec duration passage through a foil) into a mixture of coherent fs levels. Oscillations in the intensity of electric dipole lines of fixed polarization which are subsequently emitted then occur.

While the total intensity of a field-free electric dipole transition from a coherent mixture of fs levels $|JM_J\rangle$ belonging to some principal quantum state n to a group of final states n' does not oscillate in time, Macek shows that in principle the intensity of each polarization $p = 1, 0, -1$ undergoes multiperiodic oscillations. They sum to a nonoscillatory total, in contrast to cases where a Stark field is present.[2] The frequencies which occur are just the zero-field fs level-separation frequencies. Under plausible random-phase con-